A Journal of the Gesellschaft Deutscher Chemiker

Angewandte International Edition

GDCh

Chemie

www.angewandte.org

Accepted Article

Title: Core electron topologies in chemical compounds: case study of carbon vs. silicon

Authors: Daisuke Yoshida, Hannes Raebiger, Ken-ichi Shudo, and Koichi Ohno

To be cited as: *Angew. Chem. Int. Ed.* 10.1002/anie.201713108
Angew. Chem. 10.1002/ange.201713108

Link to VoR: http://dx.doi.org/10.1002/anie.201713108
http://dx.doi.org/10.1002/ange.201713108

WILEY-VCH

10.1002/anie.201713108

Core electron topologies in chemical compounds: case study of carbon vs. silicon

Daisuke Yoshida,[*,†] Hannes Raebiger,[*,†] Ken-ichi Shudo,[†] and Koichi Ohno[‡,¶]

Department of Physics, Yokohama National University, Yokohama, Japan, Institute for Quantum Chemical Exploration (IQCE), Minato-ku, Tokyo, Japan, and Department of Chemistry, Graduate School of Science, Tohoku University, Aoba-ku, Sendai, Japan

E-mail: yoshita-daisuke-rx@ynu.jp; hannes@ynu.ac.jp

Abstract

The similarities and differences of carbon and silicon have attracted the curiosity of chemists for the past few centuries. Similarities and analogies can be found in their saturated compounds, but carbon exhibits a cornucopia of unsaturated compounds that silicon (or most other elements) cannot replicate. While this *qualitative* difference is empirically well known, quantum chemistry has previously only described *quantitative* differences related to orbital overlap, steric effects, or orbital energies. We study C_2 and Si_2 and their hydrides X_2H_{2n} (X=C, Si; n = 1, 2, 3) by first principles quantum chemical calculation, and find a *qualitative* difference in the topologies of the core electrons: carbon has the propensity to alter its core electron topology when forming unsaturated compounds, and silicon has not. We draw a connection between the core electron topologies and ionization energies, and identify other elements we expect to have similarly flexible core topologies as carbon.

[*]To whom correspondence should be addressed
[†]Yokohama National University
[‡]IQCE
[¶]Tohoku University

10.1002/anie.201713108

Carbon and silicon both have four valence electrons, and thus should exhibit similar chemistries. Despite early speculations that silicon could replace carbon in arbitrary organic compounds[1] or theories of silicon-based life,[2] attempts to find silicon-equivalents for every organic compound have failed.[3] In particular, unsaturated silicon hydrides exhibit distorted (trans-bent or hydrogen-bridged) structures, whereas respective alkanes or alkynes have highly symmetric (planar or linear) structures around a central C=C or C≡C bond.[4–6] These differences have been rationalized based on e.g. the influence of the low lying 3*d* orbitals to the chemistry of silicon,[7] orbital overlap theories and steric effects,[6,8,9] or a competiton of σ and π bonds.[10–15] These previous rationalizations, however, rely on the quantization of heuristic concepts in chemistry,[16] whose quantification may be ambiguous, or out right problematic.[16–18] We pose the question, can we find a fundamental *qualitative* difference in the quantum mechanical wavefunctions that underlies the *qualitative* differences of the chemistries of carbon and silicon. To this end, our comparative first principles study of C_2 and Si_2 and their hydrides X_2H_{2n} (X=C, Si; n = 1, 2, 3) reveals different topologies for the innermost electronic shells of carbon and silicon in their unsaturated compounds. We show that carbon can form bonds that alter the topology of the innermost electronic shells, whereas silicon inner core electrons maintain their atomic like topologies in various bonding environments. Hence, for silicon, the available valence bond configurations are restricted by the core–valence orthogonality requirement, but carbon has the propensity to evade this restriction by varying the topology of its core electrons. Ionization energies of the molecules and their fragments emerge as a simple way to identify whether or not core electrons exhibit varying topologies, based on which we identify other elements expected to exhibit equally rich chemistries as carbon.

The ionization energy (IE) gives the energy required to remove the outermost electron from an atom or molecule, sc., the IE directly measures the attractive potential felt by the outermost electron (cf. electronegativity, also correlated with IE and other spectroscopic data[19,20]). To quantify this attraction, we consider this outermost electron in the field of *effective* point charges Z_{eff}, which describe the nuclear charges Z screened by all other electrons in the system (see Supplementary Information). In a typical valence bond, such a Z_{eff} is lower than for the free atom because of the

increased electron-electron repulsion due electron pairing in bonding orbitals. Such Z_{eff} for C, C_2, Si and Si_2, given in Fig. 1 (a), calculated using experimental IE,[21] show that carbon and silicon exhibit completely different behavior. For carbon, the C_2 dimer has a larger Z_{eff} than the C atom, but for silicon, Si_2 has a smaller Z_{eff} than the Si atom. Thus, the Si–Si bond increases the screening of the nuclear charge, whereas the C–C bond decreases it (here and henceforth '–' stands for a bond of unspecified multiplicity). To illustrate this difference, we plot the electrostatic potential (Figure 1 (b)–(c)) felt by the outermost electron in the field of such Z_{eff} for C_2 and Si_2 along the bond axis z, superimposed with the electrostatic potentials of the respective isolated atoms. For Si_2, this potential differs little from the superimposed isolated atom potentials, but for C_2, the electrostatic potential appears more like that of conjoined nuclei than that of two superimposed individual nuclei. Astronomy offers a simple analogy: we may have a binary star system where each star is orbited by their own planets (cf. Proxima Centauri[22]), or, one in which planets orbit both stars (cf. Kepler-47[23]).

The *conjoined nuclei* behavior alters the topology of the inner core electrons. Figure 1 (b) and (c) show the electron distribution calculated from first principles (EAS; see below and Supplementary Information) of 1s and 2s derived states for C_2 and Si_2, respectively. For Si_2, the 2s orbitals appear like spherically symmetric individual atomic orbitals, but for C_2, the 1s electrons merge and change their topology: a torus like shape electron cloud emerges around the center of the internuclear axis, separated by a node from the merged spherical electron clouds. Similar node formation in C 1s derived states is also observed for unsaturated carbon hydrides.

We study the ground state electronic structure of C_2, Si_2 and the hydrides X_2H_{2n} (X=C or Si; n = 1, 2, 3). Each of these has several low energy electronic configurations, or terms, described by the term symbol $^{2S+1}\Xi$, where $2S+1$ is the spin multiplicity (for spin S) and Ξ the symmetry species. For linear molecules Ξ is the angular momentum $\Lambda_{g/u}^{(\pm)}$ about the molecular axis, and for more complex molecules Ξ is the symmetry species. Structural parameters, such as inter-nuclear distances and bond-angles must be evaluated for each term separately. We calculate the total energy of several low-lying terms for each molecule using Hartree-Fock (HF) and complete active space

10.1002/anie.201713108

(a)

System	C	C_2	Si	Si_2
IE	11.26	11.4	8.15	7.9
Z_{eff}	1.82	2.11	2.32	1.88

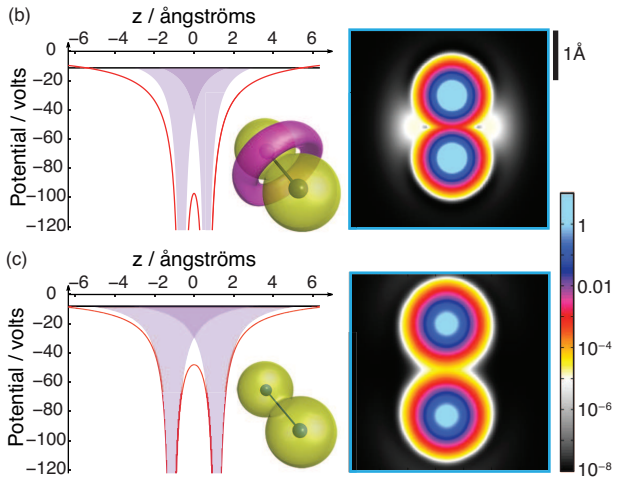

Figure 1: Nuclear attraction and core electron density distributions for C_2 and Si_2. (a) shows the ionization energies (IE)[21] in eV and effective core potentials (Z_{eff}) for C, C_2, Si and Si_2. (b) and (c) show the electrostatic potentials felt by the outermost electron for C_2 and Si_2, respectively. The red line shows the effective electrostatic potential of the diatomic molecules, and the shaded pink areas show the electrostatic potentials of the individual isolated atoms. The horizontal black line shows the IE. The right panels in (b) and (c) show core electron density distributions for 1s derived states for C_2 and 2s derived states for Si_2 calculated from first principles (EAS, see Supplementary Information), respectively. The color scale for the electron density is given on the right hand side in units of $e/\text{Å}^3$. The central insets in (b) and (c) show the symmetric (bonding) wavefunctions derived from 1s and 2s electrons for C_2 ($1\sigma_g$) and Si_2 ($2\sigma_g$). The yellow and pink wavefunction isosurfaces correspond to $\pm 0.001\sqrt{e/\text{Å}^3}$, different colors indicating opposite sign.

self-consistent field (CAS-SCF) methods implemented in the GAMESS code;[24] we include static correlation effects by full valence active spaces for all molecules (CAS henceforth), and dynamic correlation effects for C_2 and Si_2 by extended active spaces (EAS henceforth). A more accurate benchmark calculation (full configuration interaction quantum Monte Carlo) is available for the C_2 $^1\Sigma_g^+$ ground state,[25] which our EAS calculation reproduces excellently—the C_2 binding energy agrees up to 0.1 millihartree precision. For all other terms of C_2, and for Si_2, this calculation sets a new benchmark; calculated term energies are within experimental error bars where experimental references are available.[26–30] See Supplementary Information for a full account of the numerical calculation and comparison with experiment.

The fundamental difference between the chemistries of carbon and silicon becomes evident by comparison of C_2 and Si_2 molecules. C_2 has a $^1\Sigma_g^+$ ground state, and Si_2 a $^3\Sigma_g^-$ ground state, both of which are stabilized by electron correlation, but in completely different ways. Total energies calculated for the six lowest energy terms for C_2 and Si_2 are given in Fig. 2 (a) and (b). HF predicts $^3\Sigma_g^-$ ground states for both C_2 and Si_2, i.e., the highest spin and lowest angular momentum term. For the spin singlet states, HF predicts high angular momentum terms to be most stable. After including static (CAS) and dynamic electron correlation (EAS), Si_2 maintains this term ordering, but for C_2, the term ordering is completely reversed. The $^1\Sigma_g^+$ ground state has minimal spin and minimal angular momentum, and for the high spin states, the high angular momentum $^3\Pi_u$ is more stable than the $^3\Sigma_g^-$ term. The different electron correlations in C_2 and Si_2 are clarified in the following.

The representative electronic configurations for C_2 and Si_2 are given in Figure 2 (c). All but the $^1\Sigma_g^+$ have occupied $p\sigma_g$ orbitals, manifested by a charge density lobe at the center of the bond axis (see Supplementary Information) Electron correlation rearranges the electron density such that for $^1\Sigma_g^+$ we can observe an increase of electron density at the center of the bond axis, and for the other terms a depletion, as shown in Fig. 3. Naturally, a large rearrangement of electron density is associated with correspondingly large correlation energies. For C_2, these changes in electron density are more than twice as large as for Si_2, and the change is particularly large for the C_2 $^1\Sigma_g^+$ term (the

10.1002/anie.201713108

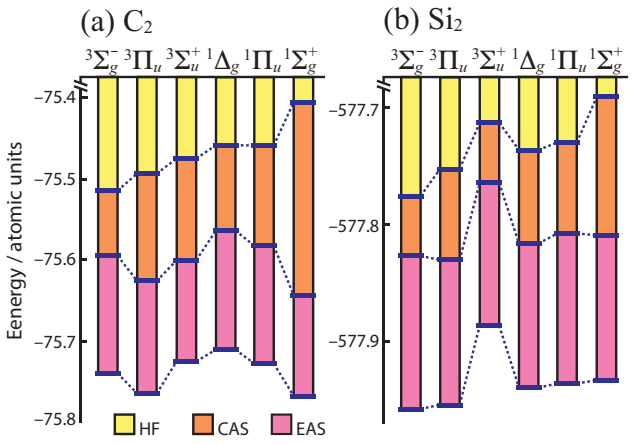

(c) Representative electronic (valence) configuration

$^3\Sigma_g^-$	$s\sigma_g^2\, s\sigma_u^2\, p\sigma_g^2\, p\pi_u^2$	$^1\Delta_g$	$s\sigma_g^2\, s\sigma_u^1\, p\sigma_g^2\, p\pi_u^2$
$^3\Pi_u$	$s\sigma_g^2\, s\sigma_u^2\, p\sigma_g^1\, p\pi_u^3$	$^1\Pi_u$	$s\sigma_g^2\, s\sigma_u^2\, p\sigma_g^1\, p\pi_u^3$
$^3\Sigma_u^+$ (C2)	$s\sigma_g^2\, s\sigma_u^1\, p\sigma_g^1\, p\pi_u^4$	$^1\Sigma_g^+$	$s\sigma_g^2\, s\sigma_u^2\, p\pi_u^4$
$^3\Sigma_u^+$ (Si2)	$s\sigma_g^2\, s\sigma_u^2\, p\sigma_g^2\, p\pi_u^1\, p\pi_g^1$		

Figure 2: Term energies for C_2 and Si_2. (a) and (b) give the total energies for the six lowest energy terms of C_2 and Si_2 using HF, CAS, and EAS. (c) shows the representative valence configurations corresponding to each term.

color scale is truncated at $\pm 0.04 e/\text{Å}^3$; isolines in the gray area indicate further increments of 0.02 $e/\text{Å}^3$). Indeed, for the C_2, this increase in electron density (cf. non-nuclear attractor[31]) is even seen in the 1s orbital derived electon density distribution (Figure 1 (b)). Such an increase of electronic density at the center of the bond axis means that correlation may strengthen C_2 $^1\Sigma_g^+$ bonding, whereas for all other terms, correlation depletes electrons from bonding orbitals. Nonetheless, for all terms of both C_2 and Si_2, the inter-nuclear distance R increases due to correlation, which speaks against bond strengthening. We quantify changes in bonding by effective bond orders (EBO, see Ref.[32] and Supplementary Information), which is the electron pair population difference between bonding and antibonding natural orbitals. For HF calculation, bond orders are always integral, but electron correlation transfers a fraction of electrons in the occupied states to virtual states, which usually implies shifting electrons from bonding to antibonding states reducing the EBO compared with HF. Indeed, the EBO given in Figure 3 (a) decrease for most terms of C_2 and Si_2 due to electron correlation effects. The only exception is the $^1\Sigma_g^+$ term of C_2, whose EBO increases due to

electron correlation, in accordance with the above described significant increase of electron density at the center of the bond axis. This increase in bond order is consistent with previous reports[33–36] that the bond of C_2 is stronger than a double bond.

The increase in EBO for the $^1\Sigma_g^+$ term of C_2, as well as its stabilization with respect to the $^3\Sigma_g^-$ HF ground state, is due to a significant increase in electro-nuclear attraction due to correlation effects. We approximate the correlation energy E^c by the difference in total energy between HF and EAS calculations, i.e., $E^c = E^{\mathrm{EAS}} - E^{\mathrm{HF}}$; $E^c_{\mathrm{stat}} = E^{\mathrm{CAS}} - E^{\mathrm{HF}}$ (orange bars in Fig 2 (a) and (b)) gives the static corretion energy, and the dynamic correlation energy follows as $E^c_{\mathrm{dyn}} = E^c - E^c_{\mathrm{stat}}$ (pink bars in Fig 2 (a) and (b)). These E^c are composed of the usual components, i.e., $E^c = T^c + V^c = T^c + V^c_{en} + V^c_{ee} + V^c_{nn}$, where T^c and V^c are kinetic and potential energy correlation energies, and the potential energy components are due to electronuclear attraction (*nn*), electron–electron repulsion (*ee*) and nucleus–nucleus repulsion (*nn*). Thanks to the virial theorem $-V/T = 2$ (which in our calculation hold to high accuracy, see Supplementary Information) we may express $E = V/2$, and $E^c = V^c/2$. Accordingly, changes in the individual potential energy components directly reflect the changes in total energy. V^c_{en}, V^c_{ee} and V^c_{nn} are shown in Figure 3 (b) and (c). For all but the $^1\Sigma_g^+$ term of C_2, the repulsion terms V^c_{ee} and V^c_{nn} are negative and lower the total energy, but this energy lowering is to some extent cancelled out by V^c_{en} of opposite sign. Only for the $^1\Sigma_g^+$ term of C_2, also V^c_{en} is negative, yielding the major total energy lowering that stabilizes $^1\Sigma_g^+$ as the ground state. Usually, an increase (or reduced screening) of the electro-nuclear attraction energy implies that electrons become more localized nearby an atomic nucleus, which would also be accompanied by a reduction of the effective atomic radius, shortening of bond length, and an increase in V_{ee} and V_{nn}. Clearly this is not the case for carbon: the increase of the electro-nuclear attraction energy is accompanied with an *increase* of the electron density distribution at the center of the bond axis (Figure 3 (a)). This lowers the total electro-nuclear potential energy because in this region, the bonding electrons feel the attraction of both nuclei, manifested by an increase in the effective nuclear charge Z_{eff} felt by the outermost electrons. Indeed, the increase of the total electro-nuclear attraction must be due to the outermost valence electrons, because the binding of

the 1s electrons for the $^1\Sigma_g^+$ term of C_2 weakens due to correlation effects (see Supplementary Information). This reduced screening of nuclear charges is caused by the change in topology of the 1s core electrons shown in Figure 1 (b): the torus like 1s charge density distribution averts direct overlap with the correlation induced increase of charge density in the center of the bond axis.

Such torus like charge density may be completely unexpected from Heitler-London or linear combination of atomic orbitals type of models, but reminds us of Bohr's model for molecules.[37] Svidzinsky *et al.* resurrect Bohr's model and show that a circular orbit at the bond center (conjoined nuclei) is lowest in energy at very small interatomic distances R, but at large R, circular orbits near each nucleus with different quantization (individual nuclei) become more stable, and simple interpolation between these solutions agrees remarkably well with accurate calculations over the entire range of R.[38] Indeed, the torus like feature emerges as R decreases below $R = 1.6$Å, and becomes larger and larger as R decreases further (See Supplementary Information), approaching the superatomic limit as $R \longrightarrow 0$. Hence, the emergence of the torus like charge density indicates a phase transition from individual nuclei to conjoined nuclei like behavior, cf. planets orbiting both stars of a twin star system.[23] For Si, both the 2s and 1s core electrons (2s shown in Figure 1 (c)) are simply a superposition of spherical atomic like s orbitals, and the Si–Si bond is better described by individual nuclei with atomic like core orbitals.

Related topological changes of core electron distributions can be observed in the unsaturated hydrocarbons C_2H_2 and C_2H_4, but not for the hydrides of silicon (see Figure 4 (a) and Supplementary Information). The nodal surfaces do not break any symmetries, so the $1\sigma_g$ orbitals of C_2, C_2H_2 and the $1a_g$ orbital of C_2H_4 maintain their original character. Outside the bubble like nodal surface for C_2, the charge density accumulates forming a torus in the central plane perpendicular to molecular axis, but for C_2H_2 and C_2H_4, charge density outside the nodal surface accumulates near the H nuclei, i.e., the $1\sigma_g$ and $1a_g$ orbitals become multicentric, engulfing also the H nuclei. This leaking of the C1s wavefunctions to the H sites *locks* the H atoms in highly symmetric (linear or planar) configurations around the central C−C bond. The core orbitals of Si_2H_2 and Si_2H_4 do

10.1002/anie.201713108

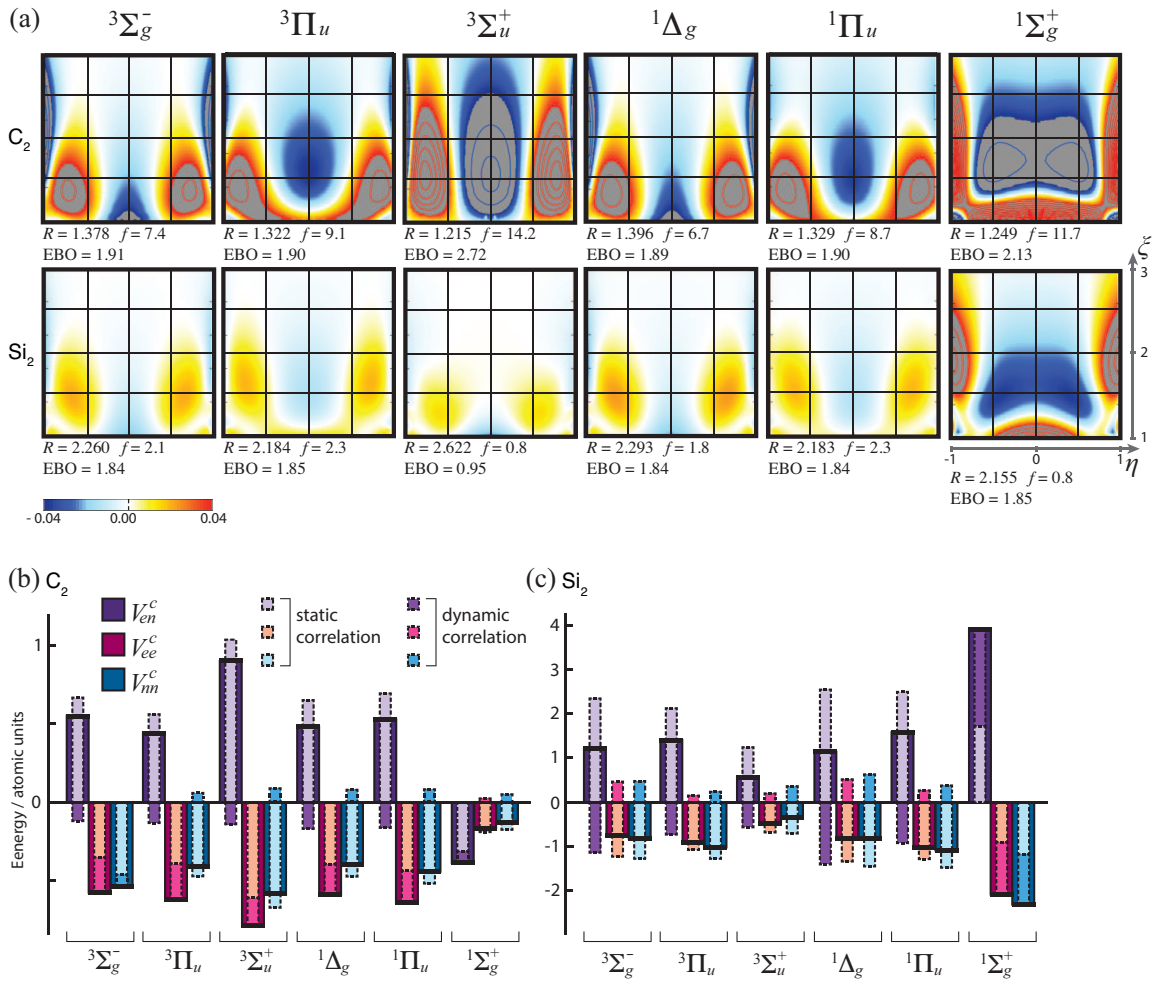

Figure 3: Correlation effects for C_2 and Si_2. (a) shows the changes in electron density distribution due to correlation effects (EAS level) compared with HF calculation on the $\xi\eta$ plane (prolate spheroidal co-ordinates, integrated about ϕ, see Supplementary Information) for each term of C_2 and Si_2 in units of $e/\text{Å}^3$ (isosurface lines beyond color scale truncation are spaced by 0.02 $e/\text{Å}^3$). The bond length R (Å), force constant f (mdyn/Å), and effective bond order EBO are given for each term below their respective panels. (b) and (c) show the correlation effects in the potential energy components V_{en}^c, V_{ee}^c and V_{nn}^c, due to static correlation (CAS) and dynamic correlation (EAS) effects.

not have such nodal surfaces, and correspondingly, their linear or planar isomers are mechanically unstable (see Supplementary Information), i.e., the core electrons prevent the formation of linear and planar isomers for Si_2H_2 and Si_2H_4, respectively. Contrariwise, ground states of C_2H_2 and C_2H_4 do not have stationary state solutions for trans-bent structures, because the H positions are *locked in* by the high symmetry $1\sigma_g$ and $1a_g$ orbitals. The type and extent of deformation of Si_2H_2 and Si_2H_4, has previously been described by valence bond mechanisms for trans-bending,[10–15] and H plays the lead role in the further deformation of Si_2H_2 into a hydrogen-bridged stucture.[39] Interestingly, these structural deformations of Si_2H_2 and Si_2H_4 have little influence on the bond order: the EBO for X_2H_{2n} suggest triple, double, and single bonds for $n = 1$, 2 and 3, respectively (see Figure 4 (a) and Supplementary Information for the hypothetical linear and planar isomers of Si_2H_2 and Si_2H_4), so when quantified by EBO, deformations have only a small influence on the electronic characteristics of the Si−Si bond.[40] When quantified by force constant f, however the Si−Si bond is very sensitive to deformations.[41,42] For C and the hypothetical linear and planar isomers of Si_2H_2 and Si_2H_4, f increases linearly with the bond order, but for the deformed (stable) Si_2H_{2n}, f hardly increases with bond order. Thus, multiple bonds characterized by linear increase in force constant f are found concomitantly with topological changes in core electronic orbitals.

Inspection of the highest occupied molecular orbitals reveals that the outermost electron of C_2H_6, Si_2H_6, and Si_2H_2 is shared with H atoms, i.e., it experiences the (unscreened) attraction of H nuclei. Thus, for all but Si_2H_4, the outermost electron experiences an incompletely screened nuclear attraction from multiple nuclei (attraction by both C nuclei for C_2H_4 and C_2H_2, and by multiple H nuclei for C_2H_6, Si_2H_6, and Si_2H_2). Indeed, only Si_2H_4 has a smaller IE than SiH_2, because in all other X_2H_{2n} molecules the outermost electron experiences a direct attraction from multiple nuclei. We may now postulate that when the highest occupied molecular orbital is a two-center bond that binds two identical fragments, an IE larger for the bonded system than for these fragments indicates topological changes in the electron core configurations. Thus, such an increased IE evidences the formation of nodes into symmetric (bonding) orbitals formed by core electrons. Based on measured values of IE[21] for the first three rows of Mendelev's table (Fig-

10.1002/anie.201713108

(a)

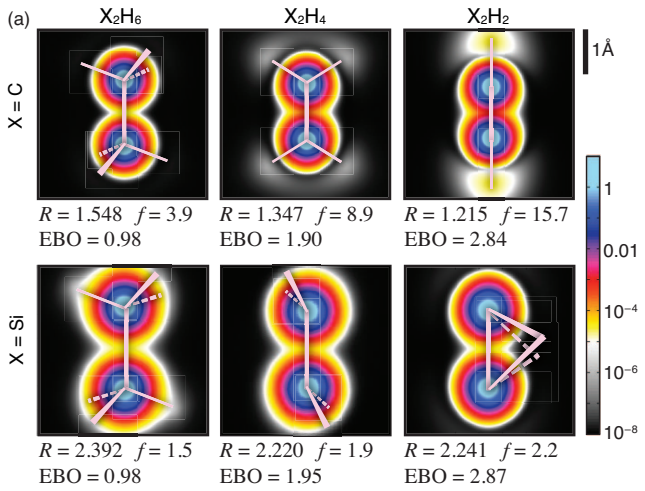

(b)

System	CH_3	C_2H_6	CH_2	C_2H_4	CH	C_2H_2
IE	9.84	11.52	10.39	10.51	10.64	11.41
System	SiH_3	Si_2H_6	SiH_2	Si_2H_4	SiH	Si_2H_2
IE	8.135	9.74	8.92	8.09	7.89	8.20

(c)

H: 13.6 H_2: 15.4	IONIZATION ENERGIES for free atoms and diatomic molecules						He: 24.5 He_2:22.2
Li: 5.39 Li_2: 5.11	Be: 9.32 Be_2: ?	B: 8.29 B_2: ?	C: 11.2 C_2: 11.4	N: 14.5 N_2: 15.5	O: 13.6 O_2: 12.0	F: 14.4 F_2: 15.7	Ne: 21.5 Ne_2:20.3
Na: 5.13 Na_2:4.89	Mg: 7.64 Mg_2: ?	Al: 5.98 Al_2: 5.4	Si: 8.15 Si_2: 7.9	P: 10.4 P_2: 10.5	S: 10.3 S_2: 9.35	Cl: 12.9 Cl_2: 11.4	Ar: 15.7 Ar_2: 14.5

Figure 4: Core electron density distributions and ionization energies of X_2H_{2n}. (a) shows core electron density distributions for 1s derived states for X=C and 2s derived states for X=Si in units of $e/\text{Å}^3$ (color scale on right hand side). The X–X bond length R (Å), force constant f (mdyn/Å), and effective bond order EBO are given for each molecule below their respective panels. (b) shows experimental ionization energies (IE)[21] in eV for X_2H_{2n} with X=C, Si and n=1,2,3 and their fragments XH_n. (c) shows experimental IE[21] for isolated atom and diatomic molecules for the first three rows of Mendelev's table. Pink frames emphasize elements for which the molecule has a larger IE than the atom.

ure 4 (c)), we predict that similar topological changes occur for N_2, P_2, and F_2 (and trivially for H_2). Another consequence of these topological changes is charge accumulation at the bond center attributed to so called *non-nuclear attractor* behavior, which indeed has been reported for N_2, P_2 and B_2,[31] supporting our above prediction of topological changes for N_2 and P_2.

Carbon is considered unique because of its capability to form a variety of stable unsaturated compounds. C_2 is at the heart of these different compounds, but always takes a slightly different guise.[43] As we show above, these guises are characterized by different nodal structures for the C 1s *core* electrons. This propensity for carbon 1s electrons to leak to neighboring nuclei or form toruses by changing their topology gives carbon the versatility to form stable uncompensated structures. Our prediction that N_2, P_2, and F_2 exhibit similar topological changes in core electron shells suggests that also nitrogen, phosphorous, and fluorine have the capability to form an equal variety of unsaturated compounds as carbon.

Acknowledgement

This work was funded by JSPS Grant-in-Aid for Scientific Research (C) No. 17K05494. We are indebted to Prof. R. Hoffmann for reading the manuscript and his help and guidance in completing this work. We thank Profs. A. Ayuela, U. Nagashima, Kaoru Ohno and M. Tachikawa and Dr. M. Goesten for many inspiring discussions.

References

(1) Wöhler, F. *Justus Liebigs Ann. Chem. Pharma.* **1863**, *127*, 257–274.

(2) Scheiner, J. *Himmel und Erde von Gesellschaft Urania* **1891**, *3*, 18–32–65–78.

(3) Kipping, F. S. *Proc. R. Soc. A* **1937**, *159*, 139–148.

(4) Jutzi, P. *Chemie in unserer Zeit* **1981**, *15*, 149–154.

(5) Raabe, G.; Michl, J. *Chem. Rev.* **1985**, *85*, 419–509.

(6) Janoschek, R. *Chemie in unserer Zeit* **1988**, *22*, 128–138.

(7) Urry, G. *Accounts Chem Res* **1970**, *3*, 306–312.

(8) Kutzelnigg, W. *Angew. Chem.* **1984**, *96*, 262–286.

(9) Malcolm, N. O. J.; Gillespie, R. J.; Popelier, P. L. A. *J. Chem. Soc., Dalton Trans.* **2002**, *0*, 3333–3341.

(10) Trinquier, G.; Malrieu, J. P. *J Am Chem Soc* **1987**, *109*, 5303–5315.

(11) Malrieu, J. P.; Trinquier, G. *J Am Chem Soc* **1989**, *111*, 5916–5921.

(12) Trinquier, G.; Malrieu, J. P. *J. Phys. Chem.* **1990**, *94*, 6184–6196.

(13) Danovich, D.; Ogliaro, F.; Karni, M.; Apeloig, Y.; Cooper, D. L.; Shaik, S. *Angew. Chem. Int. Ed.* **2001**, *40*, 4023–4026.

(14) Danovich, D.; Ogliaro, F.; Karni, M.; Apeloig, Y.; Cooper, D. L.; Shaik, S. *Angew. Chem. Int. Ed.* **2004**, *43*, 141–141.

(15) Ploshnik, E.; Danovich, D.; Hiberty, P. C.; Shaik, S. *J. Chem. Theory Comput.* **2011**, *7*, 955–968.

(16) Jansen, M.; Wedig, U. *Angew. Chem. Int. Ed.* **2008**, *47*, 10026–10029.

(17) Raebiger, H.; Lany, S.; Zunger, A. *Nature* **2008**, *453*, 763–766.

(18) Grunenberg, J. *Int. J. Quantum Chem.* **2017**, *117*, e25359.

(19) Mulliken, R. S. *J. Chem. Phys.* **1934**, *2*, 782–793.

(20) Allen, L. C. *J Am Chem Soc* **2002**, *111*, 9003–9014.

(21) Linstrom, P. J., Mallard, W. G., Eds. *NIST Chemistry WebBook, NIST Standard Reference Database Number 69*; National Institute of Standards and Technology: Gaithersburg MD, 20899, doi:10.18434/T4D303 (Retrieved 18 April 2017).

(22) Anglada-Escudé, G. et al. *Nature* **2016**, *536*, 437–440.

(23) Orosz, J. A. et al. *Science* **2012**, *337*, 1511–1514.

(24) Schmidt, M. W.; Baldridge, K. K.; Boatz, J. A.; Elbert, S. T.; Gordon, M. S.; Jensen, J. H.; Koseki, S.; Matsunaga, N.; Nguyen, K. A.; Su, S.; Windus, T. L.; Dupuis, M.; Montgomery, J. A. *J. Comput. Chem.* **1993**, *14*, 1347–1363.

(25) Booth, G. H.; Cleland, D.; Thom, A. J. W.; Alavi, A. *J. Chem. Phys.* **2011**, *135*, 084104.

(26) Ballik, E. A.; Ramsay, D. A. *Ap. J.* **1963**, *137*, 61–83.

(27) Ballik, E. A.; Ramsay, D. A. *Ap. J.* **1963**, *137*, 84–101.

(28) Douay, M.; Nietmann, R.; Bernath, P. F. *J. Mol. Spectrosc.* **1988**, *131*, 261–271.

(29) Nimlos, M. R.; Harding, L. B.; Ellison, G. B. *J. Chem. Phys.* **1987**, *87*, 5116–5124.

(30) Kitsopoulos, T. N.; Chick, C. J.; Zhao, Y.; Neumark, D. M. *J. Chem. Phys.* **1991**, *95*, 1441–1448.

(31) Terrabuio, L. A.; Teodoro, T. Q.; Rachid, M. G.; Haiduke, R. L. A. *J. Phys. Chem. A* **2013**, *117*, 10489–10496.

(32) Roos, B. O.; Borin, A. C.; Gagliardi, L. *Angew. Chem. Int. Ed.* **2007**, *46*, 1469–1472.

(33) Shaik, S.; Danovich, D.; Wu, W.; Su, P.; Rzepa, H. S.; Hiberty, P. C. *Nat. Chem.* **2012**, *4*, 195–200.

(34) Shaik, S.; Rzepa, H. S.; Hoffmann, R. *Angew. Chem. Int. Ed.* **2013**, *52*, 3020–3033.

(35) Hermann, M.; Frenking, G. *Chem. Eur. J.* **2016**, *22*, 4100–4108.

(36) Piris, M.; Lopez, X.; Ugalde, J. M. *Chem. Eur. J.* **2016**, *22*, 4109–4115.

(37) Bohr, N. *Phil. Mag.* **1913**, *26*, 857–875.

(38) Svidzinsky, A.; Chen, G.; Chin, S.; Kim, M.; Ma, D.; Murawski, R.; Sergeev, A.; Scully, M.; Herschbach, D. *Int. Rev. Phys. Chem.* **2008**, *27*, 665–723.

(39) Lein, M.; Krapp, A.; Frenking, G. *J Am Chem Soc* **2005**, *127*, 6290–6299.

(40) West, R.; Cavalieri, J. D.; Buffy, J. J.; Fry, C.; Zilm, K. W.; Duchamp, J. C.; Kira, M.; Iwamoto, T.; Müller, T.; Apeloig, Y. *J Am Chem Soc* **1997**, *119*, 4972–4976.

(41) Grunenberg, J.; Goldberg, N. *J Am Chem Soc* **2000**, *122*, 6045–6047.

(42) Grunenberg, J. *Angew. Chem. Int. Ed.* **2001**, *40*, 4027–4029.

(43) Hoffmann, R. *Am. Sci.* **1995**, *83*, 309–311.